

Washington University in St. Louis

Washington University Open Scholarship

Mechanical Engineering and Materials Science
Independent Study

Mechanical Engineering & Materials Science

5-8-2019

Effect of Reversed Flow on Rotor Blade-Flapping Stability

Joshua Norlin

Washington University in St. Louis

David Peters

Washington University in St. Louis

Follow this and additional works at: <https://openscholarship.wustl.edu/mems500>

Recommended Citation

Norlin, Joshua and Peters, David, "Effect of Reversed Flow on Rotor Blade-Flapping Stability" (2019).

Mechanical Engineering and Materials Science Independent Study. 89.

<https://openscholarship.wustl.edu/mems500/89>

This Final Report is brought to you for free and open access by the Mechanical Engineering & Materials Science at Washington University Open Scholarship. It has been accepted for inclusion in Mechanical Engineering and Materials Science Independent Study by an authorized administrator of Washington University Open Scholarship. For more information, please contact digital@wumail.wustl.edu.

Independent Study Project
MEMS 500, Section 15, Spring 2019

Joshua Norlin

Effect of Reversed Flow on Rotor Blade-Flapping Stability

Advisor: Prof. David A. Peters

Introduction:

The purpose of this project is to investigate the effect of reverse flow on blade dynamics. During a portion of the rotor revolution in forward flight, flow can actually impinge upon the trailing edge of the blade (rather than the leading edge) giving a lift reversal. This is known to have an effect on the parametric stability of the blade. The purpose of this study is to investigate that effect for various parameters, and to study what happens if an airfoil is assumed to stall in reversed flow rather than develop negative lift.

Methodology:

I used Floquet Theory applied to time marching to obtain the Floquet Transition Matrix Q and used its eigenvalues to find the characteristic exponents of the system. A positive real part of an exponent implies that an instability is present. Without reversed flow, the K and C coefficients of the system remain as K_1 and C_1 independent of azimuthal angle (i.e., independent of time). With reversed flow, the coefficients switch to K_2 or K_3 and to C_2 or C_3 depending on the location on the rotor disk, where $\psi = 0$ is aft, and $\psi = \pi/2$ is the advancing side of the disk.

Results:

The results are presented in the γ - μ plane for various values of p and B , showing the differences in the blade damping (and stability boundary) when reversed flow is included. I used $p = 0.8, 1.0$ and 1.2 and tip loss factors (B) of 1.00 and 0.98 .

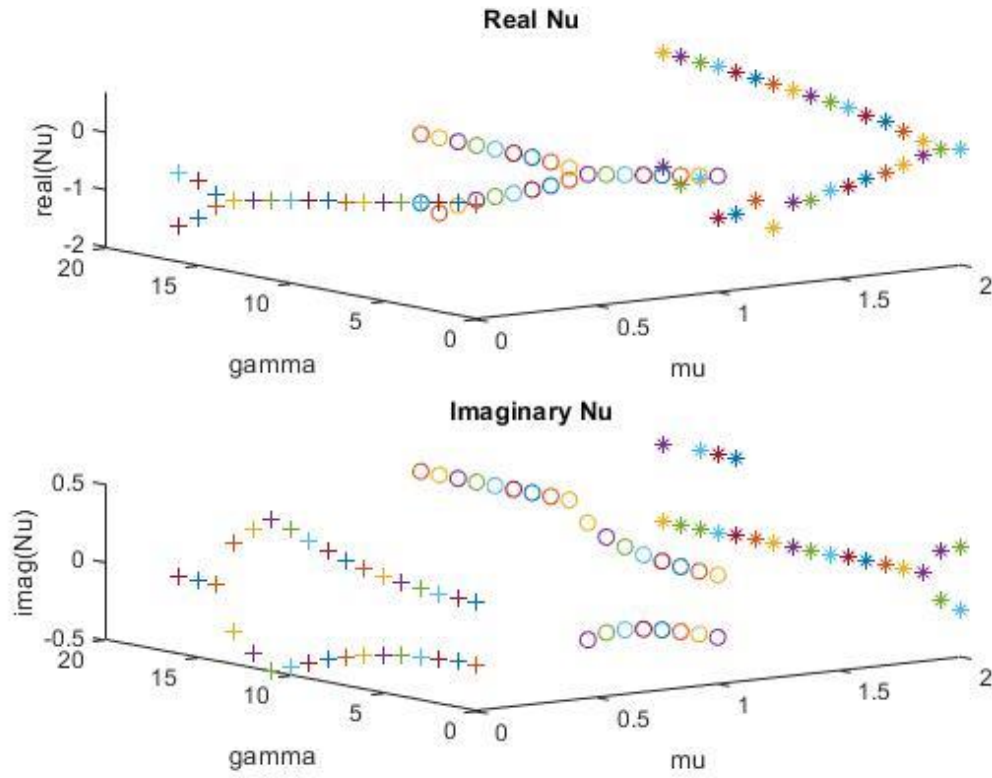


Figure 1: No Reversed Flow, $B = 0.98$, $p = 0.8$

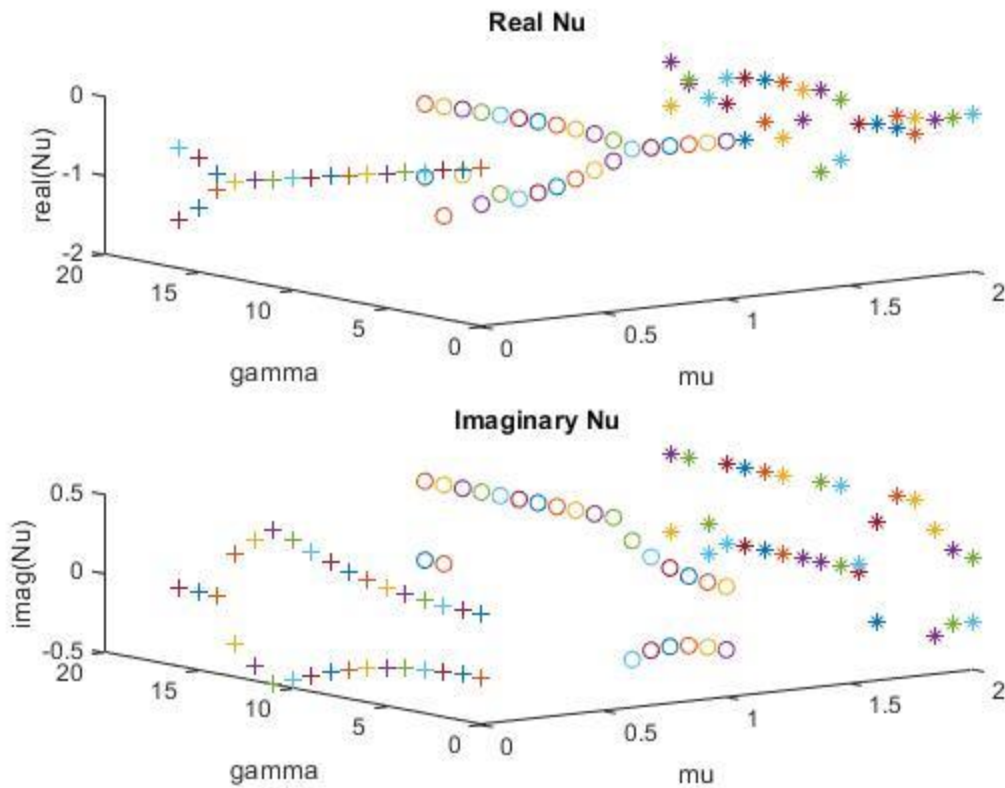


Figure 2: Reversed Flow, $B = 0.98$, $p = 0.8$

Figures 1 and 2 show results for reversed flow and no reversed flow when $B = 0.98$ and $p = 0.8$ for $0 < \mu < 2$ and for $0 < \gamma < 16$. At lower values of μ , these graphs resemble each other, but as μ increases, the instability caused by reverse flow becomes apparent in Figure 2.

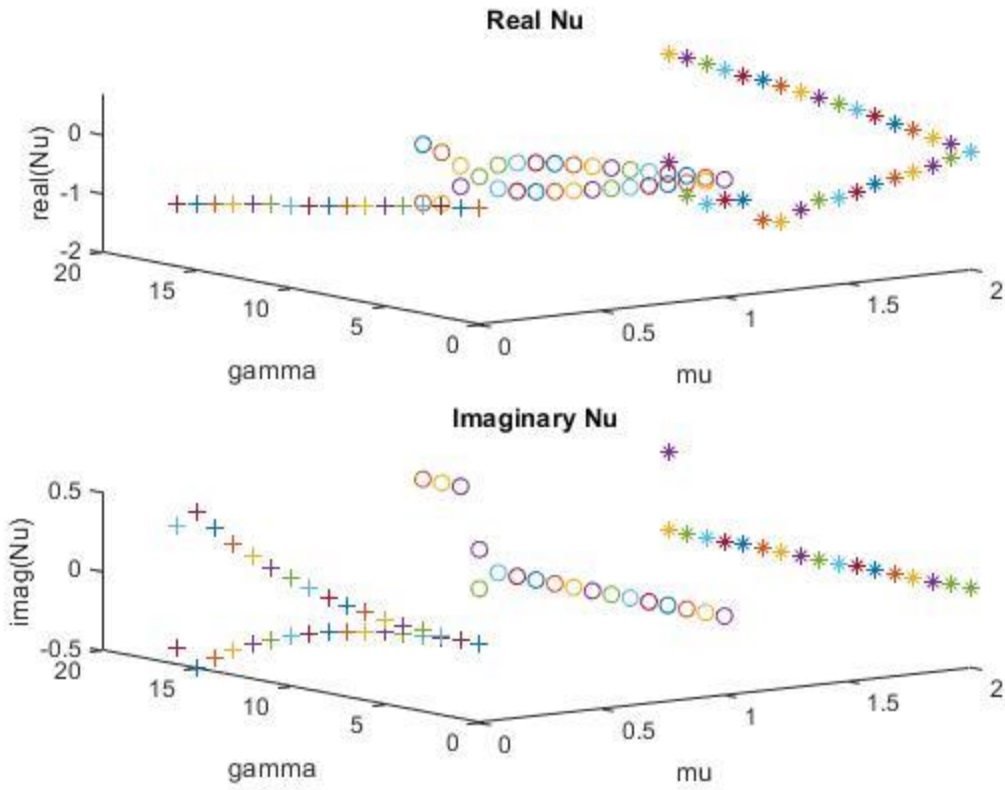


Figure 3: No Reversed Flow, $B = 0.98$, $p = 1.0$

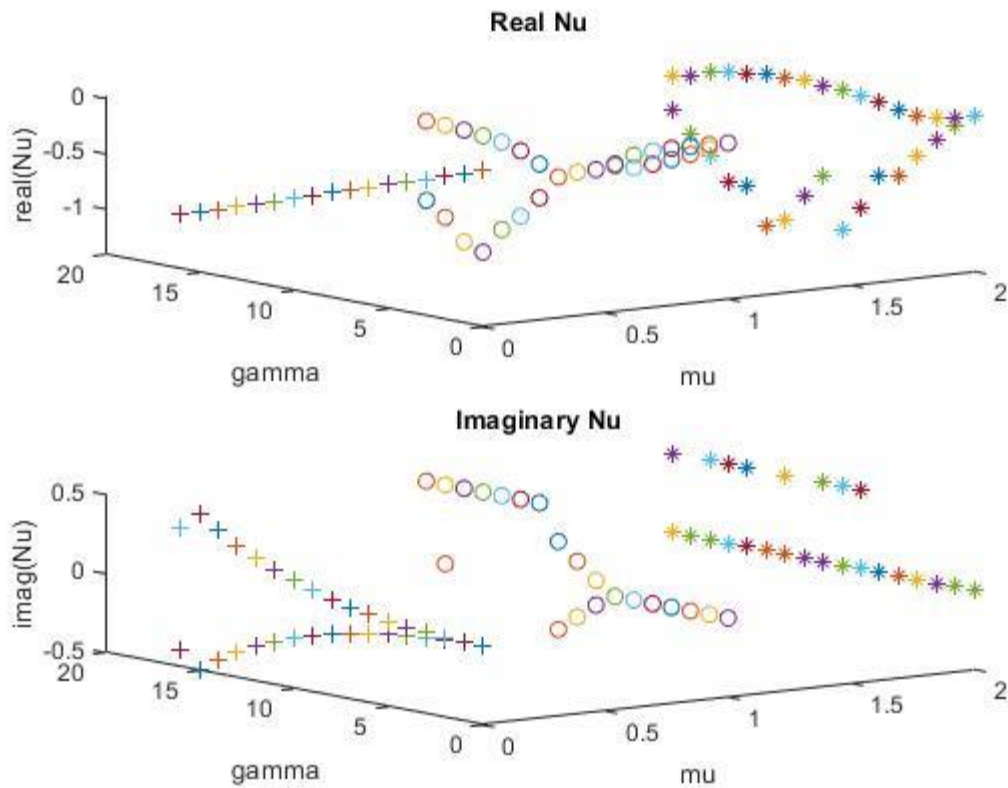


Figure 4: Reversed Flow, $B = 0.98$, $p = 1.0$

Figures 3 and 4 show results for reversed flow and no reversed flow when $B = 0.98$ and $p = 1.0$ for $0 < \mu < 2$ and for $0 < \gamma < 16$. At lower values of μ , these graphs resemble each other, but as μ increases, the instability caused by reverse flow becomes apparent in Figure 4. This is the same for Figures 1 and 2, although at the lower values of μ , the real part of Nu seems to be the same for both of the characteristic exponents, while the split remains within the imaginary portion.

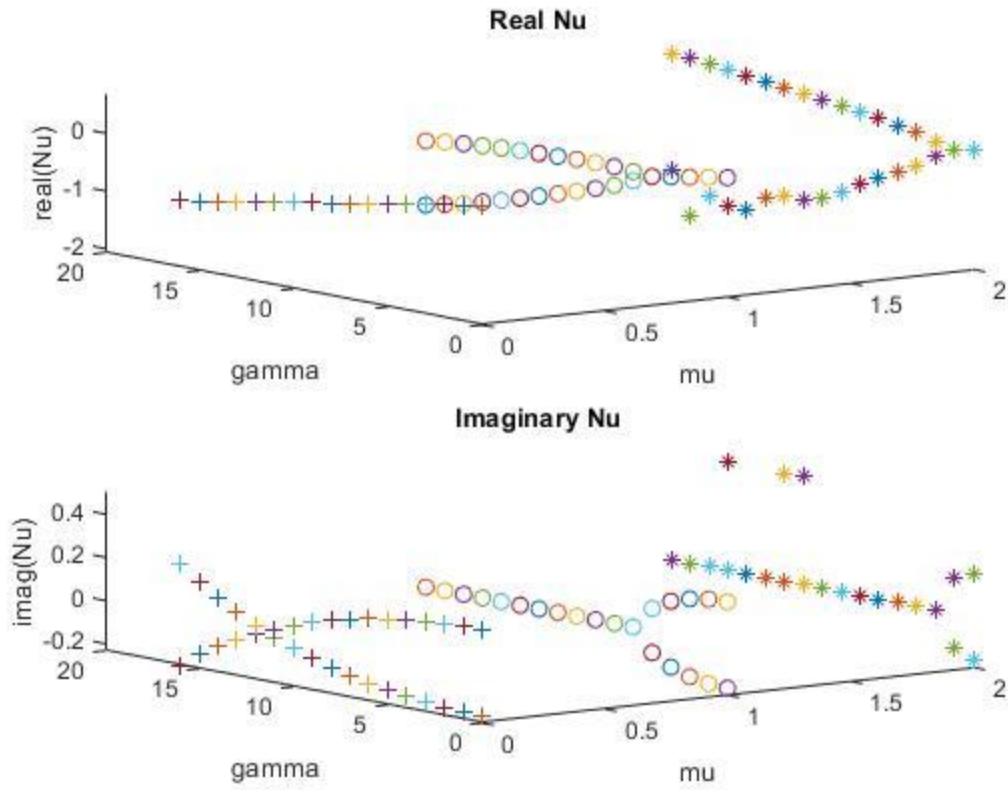


Figure 5: No Reversed Flow, $B = 0.98$, $p = 1.2$

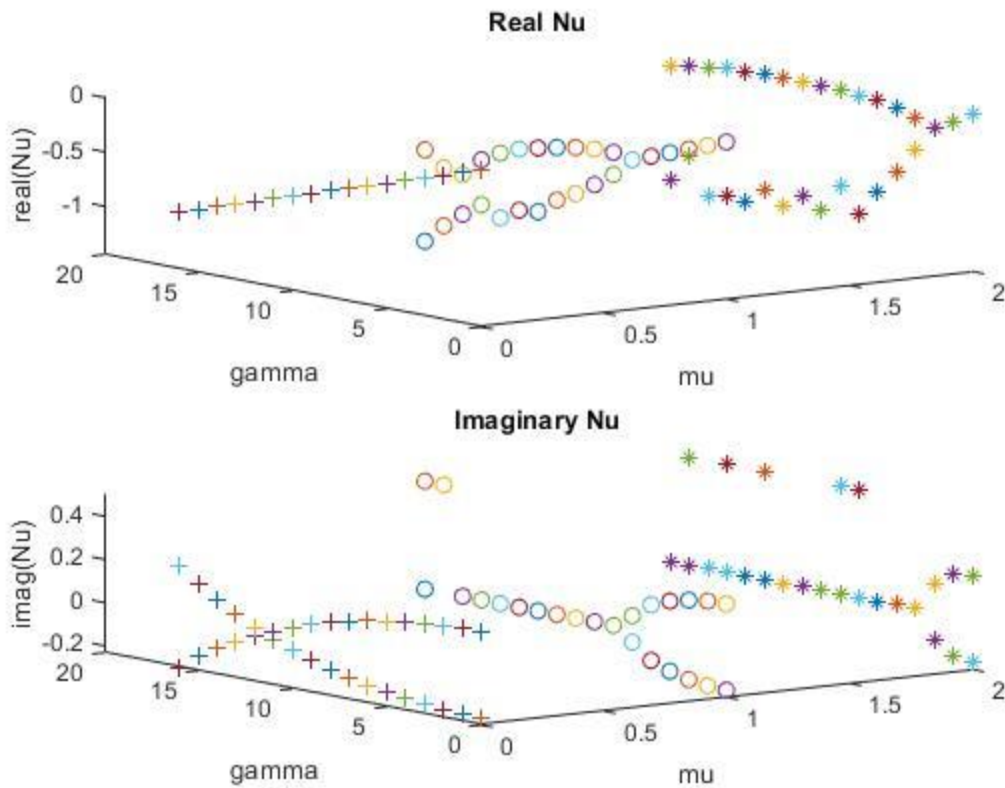


Figure 6: Reversed Flow, $B = 0.98$, $p = 1.2$

Figures 5 and 6 show results for reversed flow and no reversed flow when $B = 0.98$ and $p = 1.2$ for $0 < \mu < 2$ and for $0 < \gamma < 16$. At lower values of μ , these graphs resemble each other, but as μ increases, the instability caused by reverse flow becomes apparent in Figure 6. This is the same for Figures 1 and 2, although at the lower values of μ , the real part of Nu seems to be the same for both of the characteristic exponents, while the split remains within the imaginary portion. The split within the imaginary portion of Nu seems to be moving towards a cross pattern at the lower values of μ .

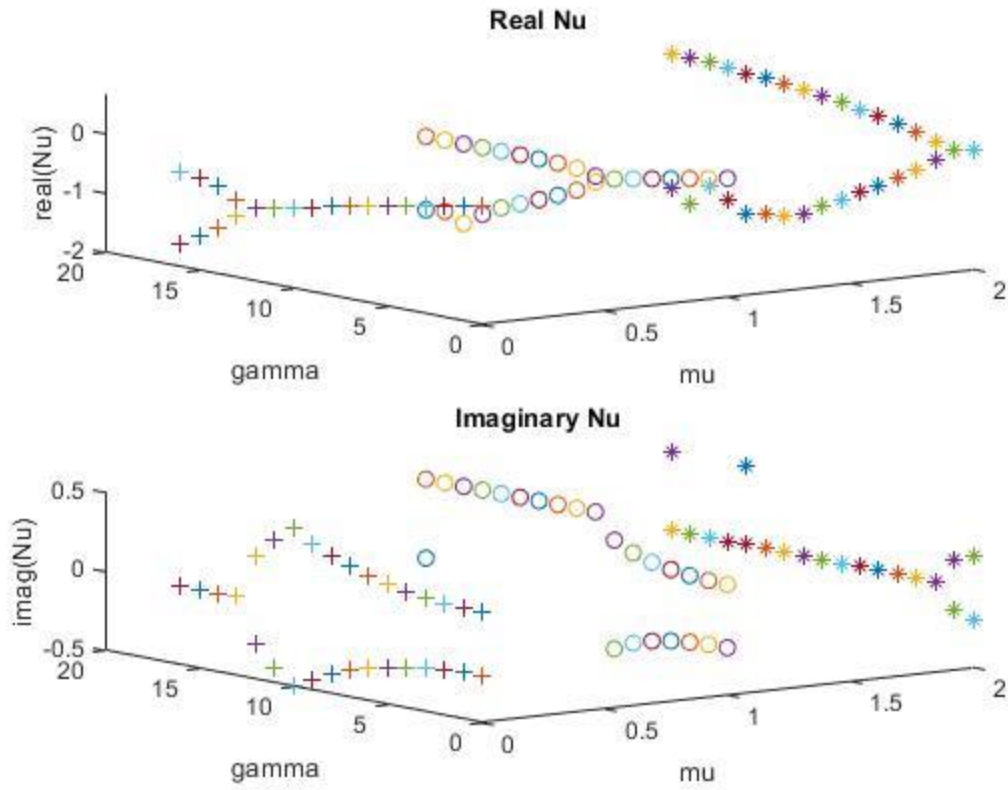


Figure 7: No Reversed Flow, $B = 1.0$, $p = 0.8$

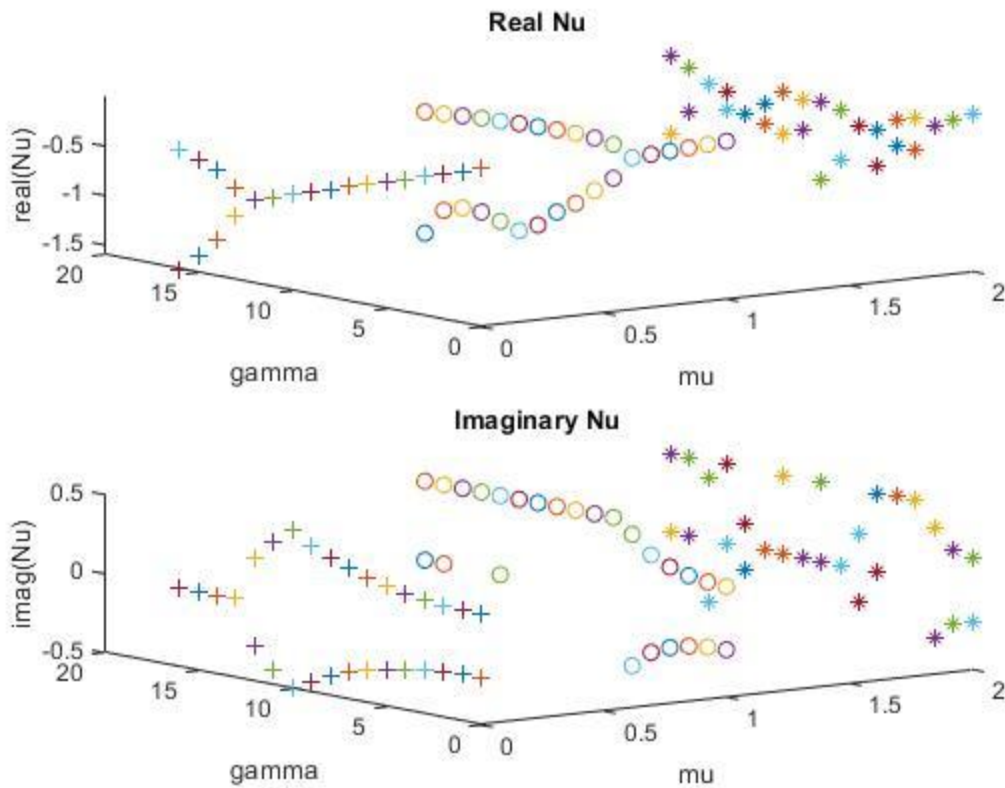


Figure 8: Reversed Flow, $B = 1.0$, $p = 0.8$

Figures 7 and 8 show results for reversed flow and no reversed flow when $B = 1.0$ and $p = 0.8$ for $0 < \mu < 2$ and for $0 < \gamma < 16$. At lower values of μ , these graphs resemble each other, but as μ increases, the instability caused by reverse flow becomes apparent in Figure 8. It is interesting to note that Figures 7 and 8 are almost indistinguishable from Figures 1 and 2, where the only difference is the value of B . It is apparent that B does not have all that great of an effect on the system for such a small change.

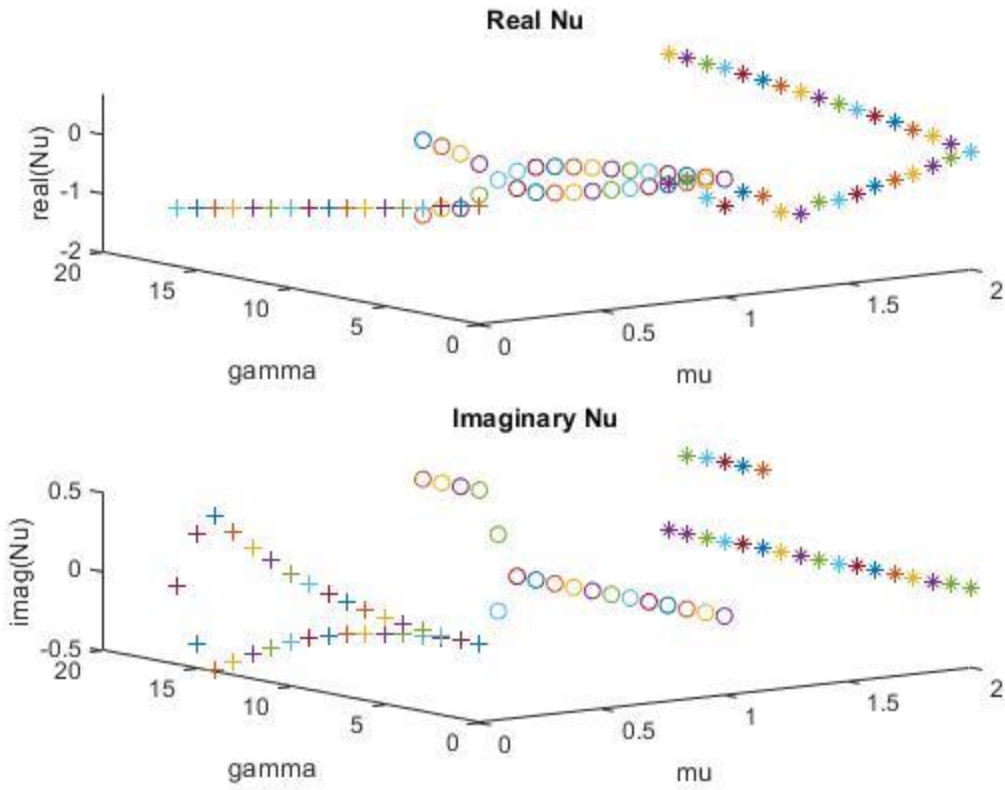


Figure 9: No Reversed Flow, $B = 1.0$, $p = 1.0$

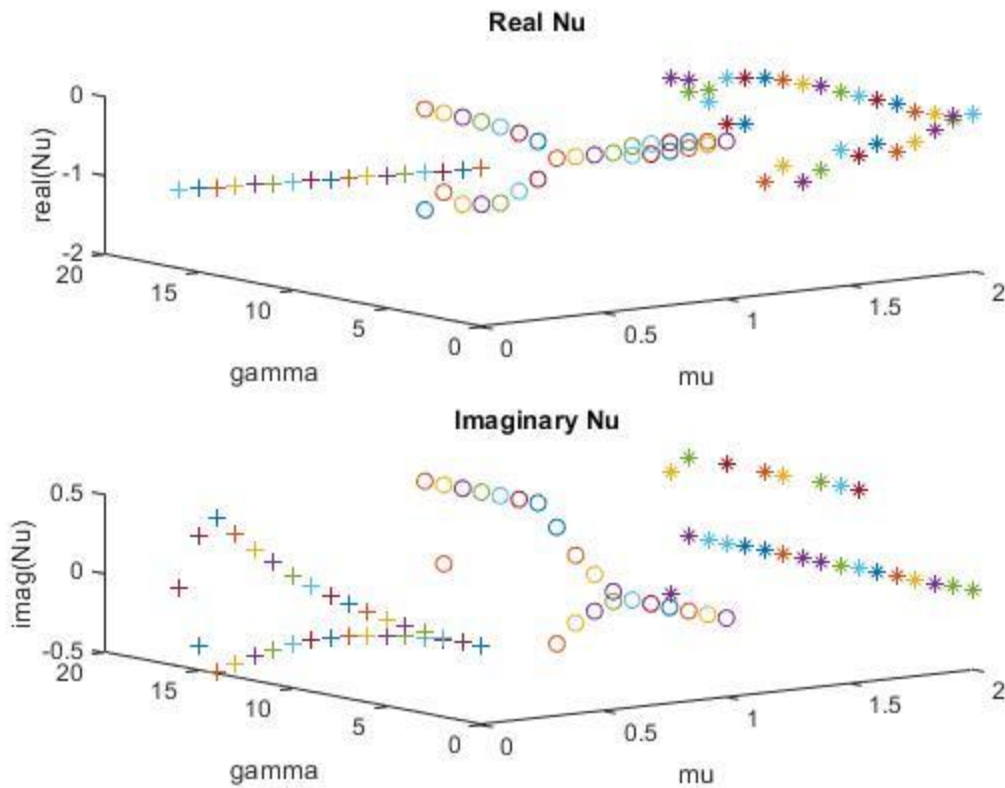


Figure 10: Reversed Flow, $B = 1.0$, $p = 1.0$

Figures 9 and 10 show results for reversed flow and no reversed flow when $B = 1.0$ and $p = 1.0$ for $0 < \mu < 2$ and for $0 < \gamma < 16$. At lower values of μ , these graphs resemble each other, but as μ increases, the instability caused by reverse flow becomes apparent in Figure 10. It is interesting to note that Figures 9 and 10 are almost indistinguishable from Figures 3 and 4, where the only difference is the value of B . It is apparent that B does not have all that great of an effect on the system for such a small change. At the lower values of μ , the real part of Nu seems to be the same for both of the characteristic exponents, while the split remains within the imaginary portion.

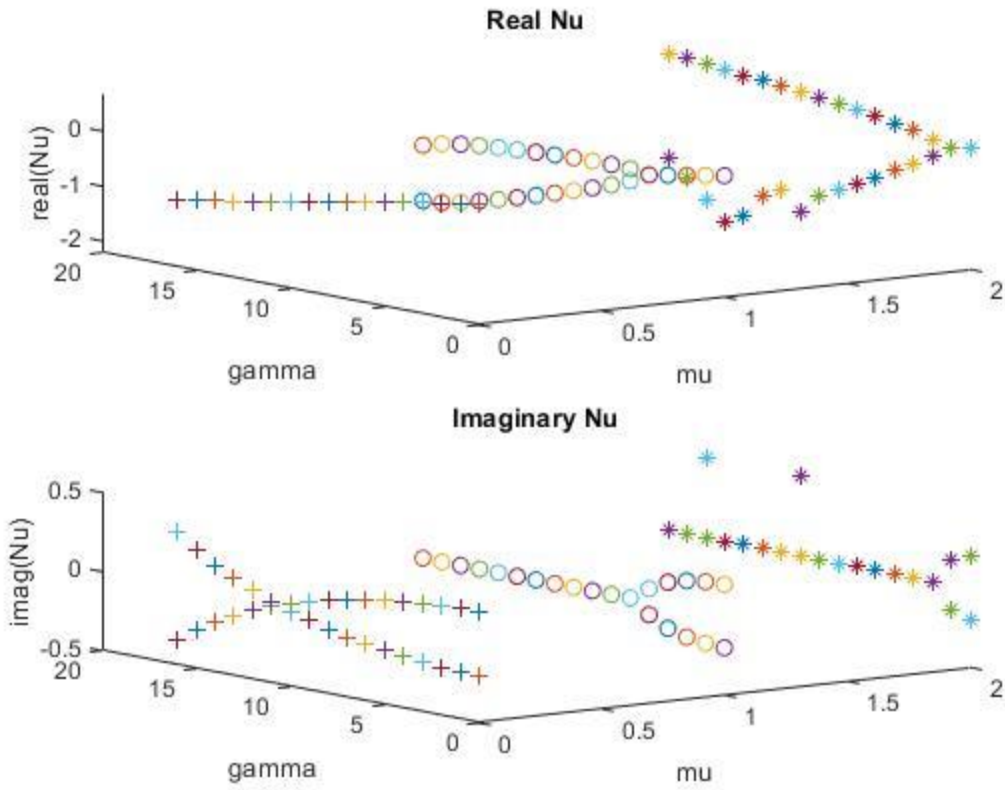


Figure 11: No Reversed Flow, $B = 1.0$, $p = 1.2$

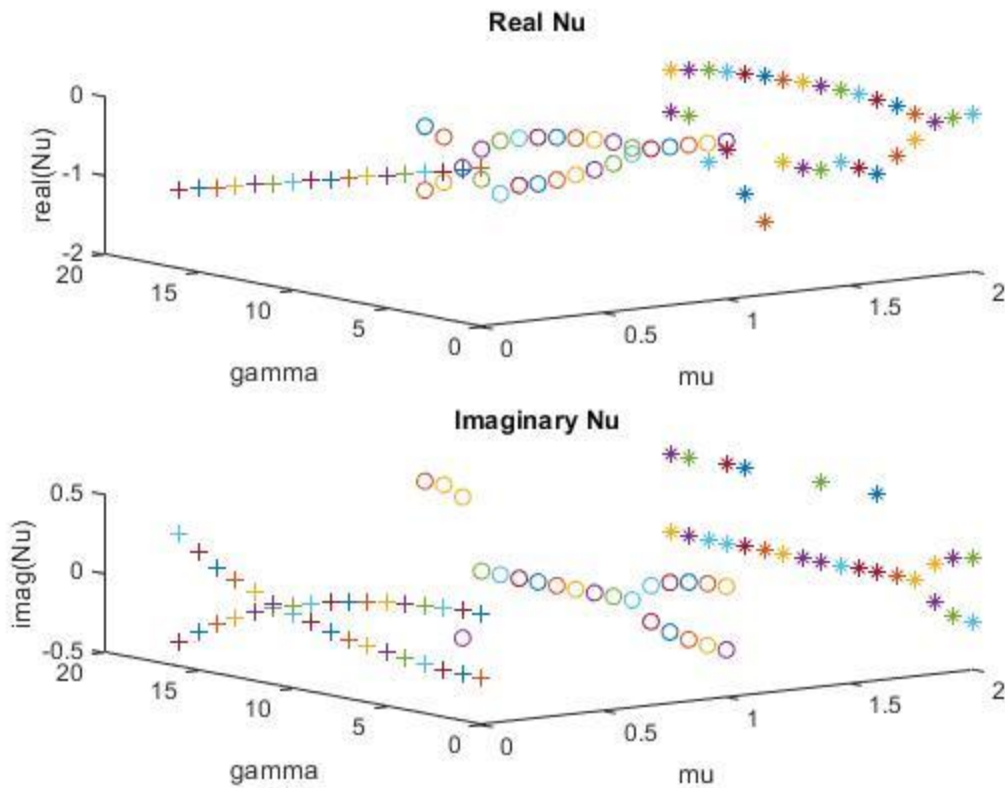


Figure 12: Reversed Flow, $B = 1.0$, $p = 1.2$

Figures 11 and 12 show results for reversed flow and no reversed flow when $B = 1.0$ and $p = 1.2$ for $0 < \mu < 2$ and for $0 < \gamma < 16$. At lower values of μ , these graphs resemble each other, but as μ increases, the instability caused by reverse flow becomes apparent in Figure 12. It is interesting to note that Figures 11 and 12 are almost indistinguishable from Figures 5 and 6, where the only difference is the value of B . It is apparent that B does not have all that great of an effect on the system for such a small change. At the lower values of μ , the real part of Nu seems to be the same for both of the characteristic exponents, while the split remains within the imaginary portion. The split within the imaginary portion of Nu seems to be moving towards a cross pattern at the lower values of μ .

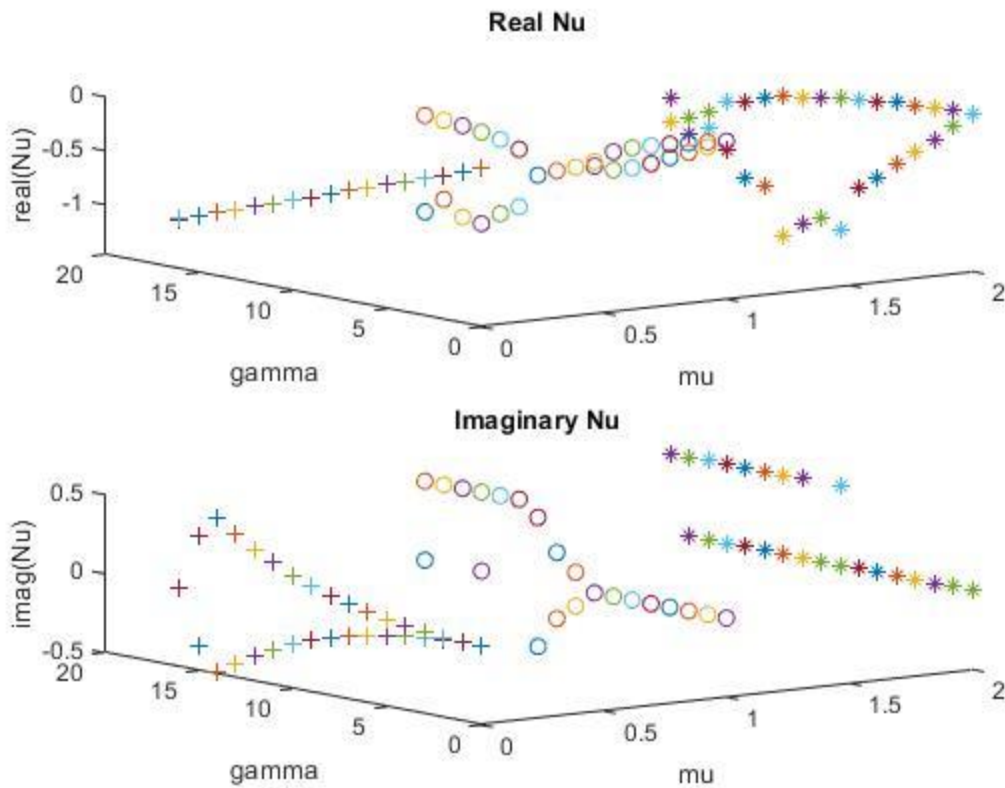


Figure 13: Reversed Flow Stall, $B = 1.0$, $p = 1.0$

Figure 13 shows the effects on Nu under stall conditions for reversed flow with $B = 1.0$ and $p = 1.0$. The results are similar to Figure 10 for reversed flow, with the instability showing earlier in μ . The main difference between these data is that for stall conditions, K_2 and C_2 are divided by 2, and $K_3 = C_3 = 0$. Attached to this report are 13 pdfs which contain the code used to obtain this data.

Discussion:

While different values of B and p were chosen for this report, only p seemed to effect any real change in the data. When the effects of reversed flow were applied, as μ increased, the system became more unstable. The stall conditions resulted in similar effects, although the instability occurred earlier on for μ . It appears that this system is dependent on the advance ratio μ for its stability.